Received: 24 August 2025 | Revised: 10 November 2025 | Accepted: 23 December 2025 | Published online: 13 January 2026

RESEARCH ARTICLE

Journal of Optics and Photonics Research
2026, Vol. 00(00) 1–11
DOI: 10.47852/bonviewJOPR62027361

BON VIEW PUBLISHING

Evaluation and Characterization of the Optical Properties of NBR Rubber/N220 Granular Carbon Black Composites

K. Alfaramawi[1,*], S. Abboudy[1], L. Abulnasr[1], S. Ebrahim[2] and Ahlam K. Yousif[1]

[1] *Department of Physics, Faculty of Science, Alexandria University, Egypt*

[2] *Department of Materials Science, Institute of Higher Studies and Research, Alexandria University, Egypt*

Abstract: This study investigates the optical and dielectric properties of nitrile butadiene rubber (NBR) reinforced with varying concentrations of N220 carbon black (CB). Ultraviolet (UV)–visible spectroscopy, in the range of 200–800 nm, was used. The optical spectrum showed a high absorption peak at approximately 220 nm, indicating that the material is suitable as a strong absorber of ultraviolet radiation. The direct optical band gap decreases slightly from 5.55 eV to 5.34 eV as CB content increases. The Urbach energy values, around 1.5 eV, suggest the formation of structural disorder and band tail states induced by CB–rubber interfacial interactions. The optical parameters such as extinction coefficient and refractive index exhibit characteristic variations around 220 nm, corresponding to strong absorption and high photon–carrier coupling. Dispersion behavior, interpreted through the Wemple–DiDomenico and Sellmeier models, reveals consistent variations in the effective oscillator energy, dispersion energy, and oscillator length strength. Dielectric analysis demonstrates that both the static and high-frequency dielectric constants are sensitive to CB loading, while the real part of the dielectric constant dominates over the imaginary component across the spectrum. Generally, the optical and dielectric findings demonstrate that the incorporation of N220 CB substantially modifies the energy band structure, optical dispersion, and charge carrier dynamics of NBR composites. These characteristics suggest their promising potential for optoelectronic and UV-sensing applications, where tunable optical absorption and dielectric response are critical.

Keywords: NBR, N220 carbon black, optical and dielectric properties, Urbach energy

1. Introduction

Nitrile butadiene rubber (NBR), a synthetic copolymer comprised of acrylonitrile (CH_2=CH–CN) and butadiene (CH_2=CH–CH=CH_2), is widely used in industrial and automotive applications, including oil seals, hoses, belts, and brake linings [1, 2]. To further enhance its functional performance, various reinforcing fillers are incorporated into NBR matrices. Among these, carbon black (CB) remains one of the most ubiquitous conductive and reinforcing additives in rubber composites [3, 4]. One commonly used grade is N220 CB, a fine amorphous form of carbon typically employed in high-performance rubber formulations. N220 exhibits stability, excellent UV and light fastness, chemical inertness, and a high burning point (above 400 °C) [5–7].

In the last decades, the scope of research on polymer–filler composites has broadened, with increased interest in linking optical, dielectric, and electronic behaviors to microstructure. For instance, Taha et al. [8] explored the optical characteristics of NiO-doped polyvinyl chloride (PVC/NiO), revealing that the addition of NiO nanoparticles resulted in increased refractive index and normalized absorption. Alfaramawi [9] examined the optical properties of butyl rubber/general purpose furnace CB composites at varying CB concentrations. Due to the high ultraviolet (UV) absorption capability of the CB filler, most of the incident UV light was absorbed within the composites. Samthong et al. [10] analyzed the morphology, thermal, and tensile properties of poly(lactic acid) blends that comprised NBR with different acrylonitrile contents, both with and without dynamic vulcanization facilitated by dicumyl peroxide. Parvathi et al. [11] investigated the optical and thermal stability, alongside temperature-dependent electrical properties, of chlorinated natural rubber (Cl-NR) combined with zinc ferrite ($ZnFe_2O_4$) nanocomposites. Their findings suggested that doping Cl-NR with $ZnFe_2O_4$ led to a reduction in bandgap energy and enhanced thermal stability of the rubber nanocomposites as nanoparticle content increased. Rejani and Beena [12] studied the optical properties of manganese oxide/polyindole (Mn_2O_3/PIND) hybrid structures, observing that the optical absorption in the UV–visible (UV–Vis) region indicated that polyindole possesses a direct bandgap, which narrows from 4.4 eV to 3.3 eV with the formation of the hybrid.

Recently, Naser et al. [13–15] studied the optical properties of foil nanocomposites using three types of neat polymers: polystyrene, poly (methyl methacrylate), and polyvinyl alcohol mixed with zinc oxide, silver, and aluminum nanoparticles. All foil nanocomposites exhibited high UV absorption but low visible

***Corresponding author:** K. Alfaramawi, Department of Physics, Alexandria University, Egypt. Email: kalfaramawi@alexu.edu.eg

absorption, especially when mixed with Ag and Al nanoparticles in the 200–400 nm range. The results showed a decreasing energy band gap from 4.40 eV to 3.7 eV as the concentrations of Al nanoparticles increased. Alam [16] reported and reviewed the methods of filler dispersion in rubber composites for optimizing the properties of rubber composites.

Despite these advances, comprehensive studies linking UV–Vis absorption behavior, optical band structure (band gap and Urbach tails), refractive index dispersion, and dielectric response in rubber/CB systems remain relatively scarce. Here, we address this gap by systematically investigating NBR/N220 composites with varying CB loadings, focusing on their optical absorption (200–800 nm), optical dispersion, and dielectric characteristics. The novelty of this work lies in presenting a comprehensive optical–dielectric investigation of NBR composites reinforced with nano-sized N220 CB through combined evaluation of the optical band gap, Urbach energy, extinction coefficient, refractive index (via Wemple–DiDomenico (WD) and Sellmeier models), and dielectric parameters including permittivity, relaxation time, plasma frequency, and loss functions. This work provides a unified framework linking filler concentration to charge carrier dynamics and photon–material interactions. The systematic correlation between optical and dielectric properties in NBR/N220 composites can effectively tune both the optical band structure and dielectric polarization behavior, offering a new pathway for developing multifunctional elastomeric materials for advanced optoelectronic, photothermal, and UV-sensing applications.

2. Experimental

2.1. Materials

The materials used in this study are medium-grade NBR with acrylonitrile content 30–35% (supplied by Transport and Engineering Co., Alexandria., Egypt), Intermediate Super Abrasion Furnace CB of grade N-220 (supplied by Alexandria Carbon Black Co., Alexandria, Egypt), zinc oxide (ZnO) of purity 99.5% (supplied by Aldrich Company, Germany) as activators, stearic acid of purity 97–99% acts as dispersing/activating fatty acid (supplied by Aldrich Company, Germany), fine pale yellow sulfur (S) powder of purity 99% as a vulcanizing agent (supplied by Aldrich Company, Germany), 2'-dibenzothiazole disulfide (MBTS) $C_{14}H_8N_2S_4$ of purity 98% as an accelerator, dioctyl phthalate (DOP) of purity 99% as a processing oil, and N-isopropyl-N'-phenyl-p-phenylene diamine (IPPD4020) of purity 99% as an antioxidant, antiozonant, and antiflex.

2.2. Methods

The NBR primary matrix with content of 100 phr (part per hundred parts of rubber by weight in grams), 2 phr of stearic acid, 5 phr of zinc oxide, 2 phr of sulfur, 10 phr DOP processing oil, 2 phr of MBTS accelerator, and 1 phr of IPPD4020 antioxidant/antiozonant were combined thoroughly with N220 CB of concentrations 50, 60, 70, 80, 90, and 100 phr.

Two roll mills with dimensions of 300 mm in length and 150 mm in diameter, a slow roll speed of 18 rpm, and a 1.4 gear ratio were employed in this process. The mixing process was carried out according to the "Compounds and Prepared Standard Vulcanized Sheets (ASTM D 3182)" [17, 18]. Following the mixing process, the rubber composites were allowed to rest for a full day prior to vulcanization. Vulcanization was carried out using an electrically heated platen hydraulic press, which maintained the temperature at 150 ± 2 °C and applied a pressure of 15 MPa for 15 minutes. The resulting sheets were shaped as 5 × 5 cm² with a thickness of 1 mm. From these sheets, small samples measuring 1 × 1 cm² were cut for characterization, and each sample was coded according to its CB content, labeled as N50, N60, N70, N80, N90, and N100, as the N220 CB content is 50, 60, 70, 80, 90, and 100 phr, respectively.

2.3. Optical characterization techniques

UV–Vis spectroscopy was utilized to measure absorbance and reflectance over a wavelength range of 200–800 nm, using an EVO300 PC model spectrophotometer.

3. Results and Discussion

3.1. Optical characterization

The reflectance spectrum of a material provides valuable insights into its optical and dielectric characteristics. Figure 1(a) illustrates the relationship between measured reflectance (*R*) and

Figure 1
Variation of reflectance with incident photon wavelength of NBR/N220 composites with various N220 CB concentrations: (a) from 200 to 800 nm wavelength range and (b) in the UV range of the electromagnetic spectrum

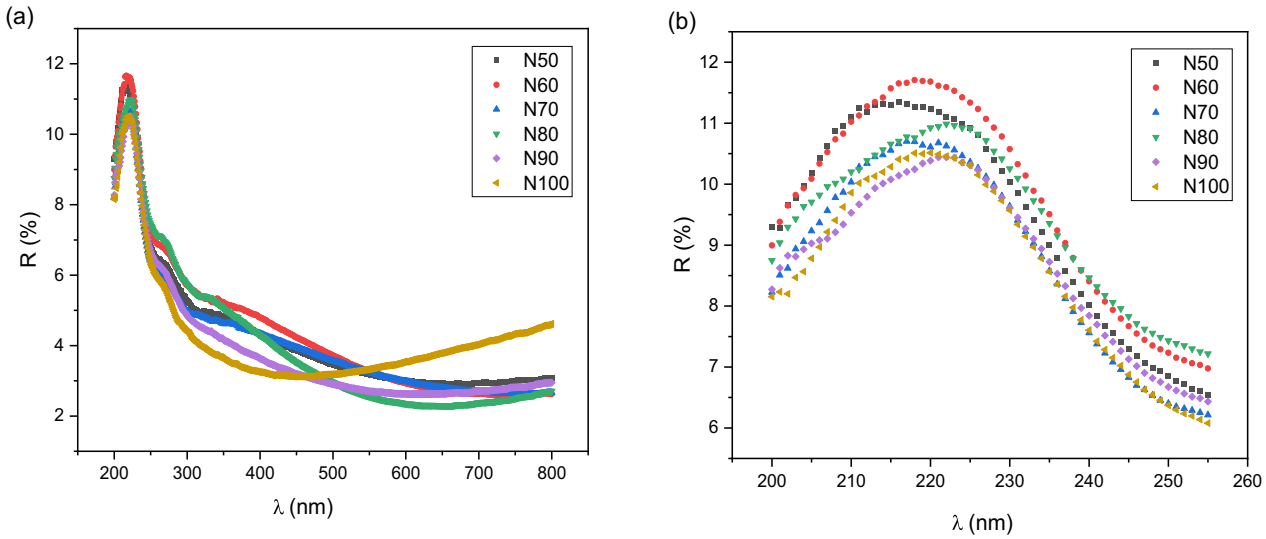

Figure 2
Kubelka–Munk function F(R) versus photon wavelength in the range 200–260 nm of NBR/N220 CB composites at various CB concentrations

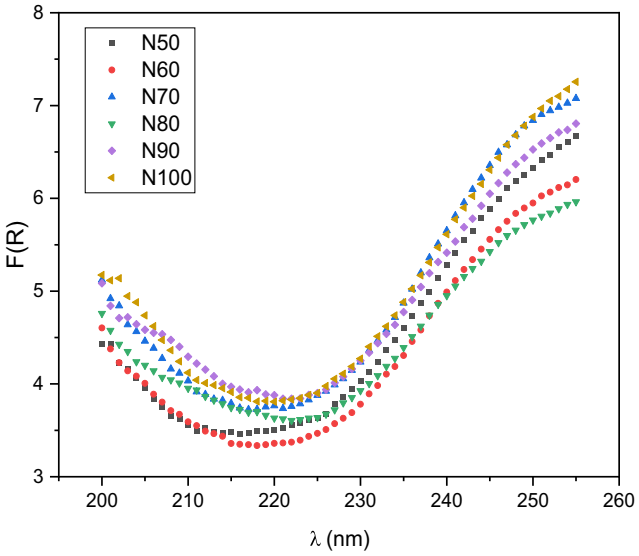

Figure 3
Plot of $(F(R).E)^2$ versus photon energy to estimate the direct optical band gap of NBR/N220 composites with various N220 CB concentrations

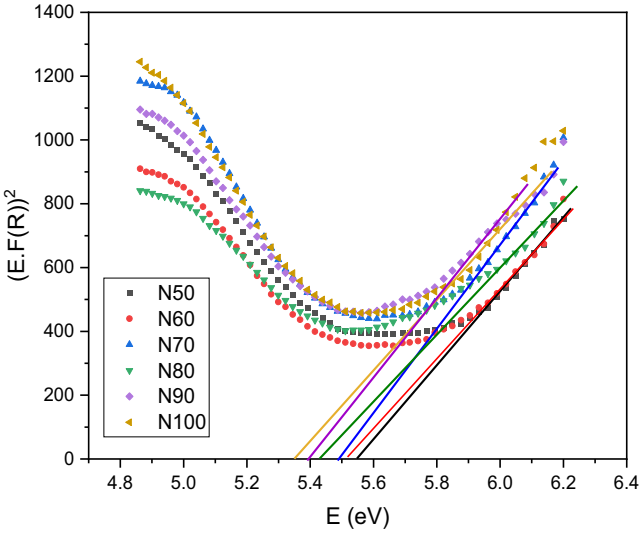

incident photon wavelength from 200 to 800 nm for various NBR/N220 composites, while Figure 1(b) shows such a graph in the UV range.

The reflectance spectra of the NBR/N220 composites show a pronounced absorption-like edge in the UV (≈ 300 nm), followed by a broad minimum in the visible region (≈ 400–600 nm) and a weak upturn toward the near-IR for the highest filled sample. This behavior is consistent with strong electronic transitions in the polymer (π–π^* from C=C/C≡N groups) combined with broadband absorption from the graphitic domains of the CB; the addition of N220 progressively attenuates the reflectance across the measured range, indicating increased light absorption and enhanced multiple scattering from the filler network [19].

Throughout all wavelengths, reflectance behavior demonstrates a pattern that is related to absorbance. It is convenient to convert the diffuse reflectance (DR) data to an effective absorption function. The theory that makes it possible to use DR spectra was proposed by Kubelka and Munk [20]. Originally, they proposed a model to describe the behavior of light traveling inside a light-scattering specimen from the relation:

$$F(R) = \frac{(1-R)^2}{2R} \tag{1}$$

where ($R = R\%/100$) and F(R) is the so-called remission or Kubelka–Munk function. The Kubelka–Munk function in diffuse reflection represents the absorption coefficient. Figure 2 shows F(R) versus wavelength (in the range 200–260 nm) for NBR/N220 composites of various CB content. Since F(R) represents the Kubelka–Munk function, it's proportional to the absorption coefficient, so this graph highlights how optical absorption evolves with CB content in the UV region.

The variation of the Kubelka–Munk function F(R) with wavelength for the NBR/N220 composites (Figure 2) reveals a noticeable absorption feature in the deep-UV range (200–260 nm). All samples exhibit a distinct minimum near 220 nm, followed by a sharp increase in F(R) toward shorter wavelengths, corresponding to the strong electronic transitions associated with π–π^* excitations in the conjugated C=C and C≡N groups of the NBR matrix. With increasing CB (N220) loading, F(R) values rise systematically across the spectrum, reflecting enhanced absorption and scattering due to the formation of a conductive filler network. This trend confirms the light-attenuating nature of N220, where graphitic domains introduce additional π–π^* transitions and localized electronic states within the polymer band structure [21]. The upward shift in F(R) intensity from N50 to N100 suggests an increasing density of absorbing centers and interfacial charge-transfer interactions between the rubber matrix and CB aggregates.

Tauc's equation provides a method to establish the relationship between photon energy and absorption coefficient (represented by F(R)), expressed as follows [22]:

$$F(R).E = C(E - E^{opt})^m \tag{2}$$

In this equation, E represents the photon energy, (E^{opt}) denotes the optical band gap, C is a constant that does not depend on energy, and m indicates the type of optical transition. Specifically, m takes the value of ½ for direct allowed transitions and 2 for indirect allowed transitions. To determine the direct optical energy gap (E^{opt}) of the NBR-N220 composites, Equation (2) is utilized. Figure 3 presents a plot of $(F(R).E)^2$ versus photon energy, from which the direct optical band gap is estimated by extrapolating the linear portion of the curve at the absorption edge.

The estimated direct optical energy gap values for all NBR/N220 samples are presented in Table 1. Notably, there is a slight decrease in the direct optical band gap from 5.55 to 5.34 eV as the CB content increases. This trend can be logically attributed to the enhanced conductivity of the composite with a higher concentration of CB. The inclusion of CB in NBR rubber can alter the material's absorption coefficient and energy structure as a result of the interactions between the rubber matrix and the CB particles. A significant alteration in the material is the formation of band tail energy, also known as Urbach energy, which is primarily attributed to localized states within the band gap associated with semicrystalline materials [22]. The relationship between the

absorption coefficient (represented by F(R)) and the incident photon energy is described by the Urbach relation [23]:

$$F(R) = \alpha_0 \, exp\left(\frac{E}{E_u}\right) \tag{3}$$

where (E_u) represents the Urbach energy and (α_0) denotes the Urbach constant. Consequently, plotting ($ln\ F(R)$) against (E) enables the determination of both parameters through Equation (3). Figure 4 illustrates this graph for the various NBR/N220 composites. E_u is determined from the inverse of the slope of the straight-line portion, while α_0 is found by locating the intercept on the vertical axis. Table 1 lists the estimated values of both Urbach energy and Urbach constant for each sample.

It is noteworthy that Urbach energy has values between 1.1 and 1.6 eV for the NBR/N220 composites. This range appears significantly higher than those values reported in previous studies of similar rubber/CB systems [24, 25]. This is probably because the introduction of CB particles may disturb the molecular ordering of NBR chains. Additionally, the interfaces between CB and rubber matrix may create localized states and potential fluctuations. Also, poor filler dispersion or strong CB agglomeration enhances this disorder, and this results in increased density of localized states leading to broader Urbach tail and consequently higher E_u [26]. On the other hand, CB contains sp^2 domains, defective graphitic structures, and amorphous carbon regions. The electronic transitions in these regions (π–π^*, sp^2–sp^3 disorder) add

Figure 4
Urbach plot of ln F(R) against photon energy of the different NBR/N220 composites

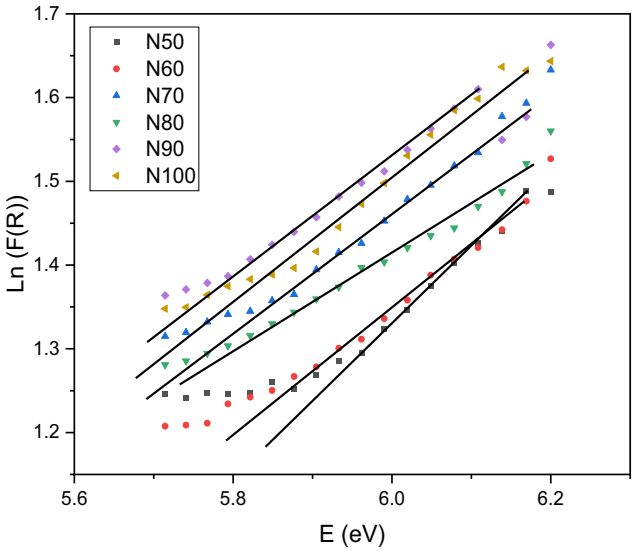

Figure 5
Extinction coefficient of NBR/N220 composites with varying N220 CB concentrations versus photon energy

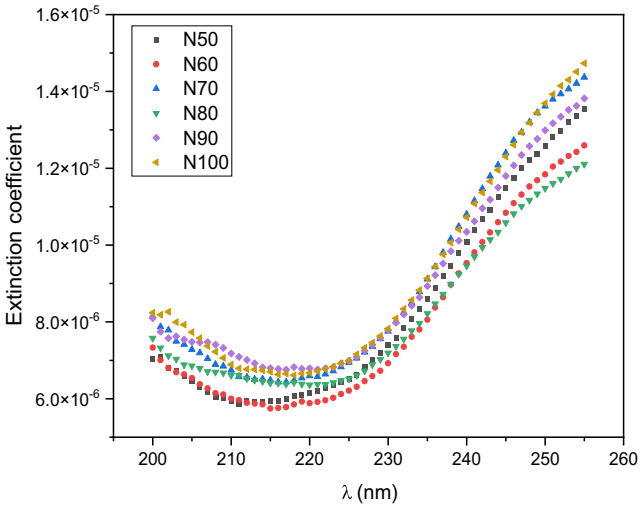

broad absorption features extending into the visible region. These additional localized electronic states overlap with the rubber band tail, effectively broadening the exponential absorption region [27].

A crucial factor associated with absorption measurements is the extinction coefficient (k), also referred to as the absorption index. This coefficient quantifies the percentage of electromagnetic waves lost due to absorption and scattering over a unit length of the medium. The extinction coefficient can be calculated using the following relation [22]:

$$k = \frac{F(R).\,\lambda}{4_\pi} \tag{4}$$

Figure 5 illustrates how the extinction coefficient varies with the wavelength of incident photons in the UV range for the investigated NBR/N220 composites at various concentrations of N220 CB. The graph shows that the extinction coefficient initially increases as the wavelength increases, reaching a maximum at around 220 nm, which is close to the absorption edge. Beyond this point, k continues to decrease with further increases in wavelength. Notably, there is a clear correlation between the trends of both the extinction coefficient and absorbance in the UV range, particularly at 220 nm. The corresponding energy level is near the energy gap of the NBR rubber composites, indicating a significant absorption of radiation energy at this juncture. Consequently, this characteristic suggests possible potential use for utilizing these rubber systems in practical applications as sensors and actuators for detecting and absorbing ultraviolet electromagnetic waves.

Table 1
Direct optical band gaps, Urbach energy, and Urbach constant of NBR/N220 composites with various N220 CB concentrations

Parameter	Samples					
	N50	N60	N70	N80	N90	N100
E^{opt} **(eV)**	5.55	5.52	5.49	5.44	5.39	5.34
E_u **(eV)**	1.52	1.45	1.37	1.61	1.41	1.11
α_o **(cm^{-1})**	0.073	0.062	0.057	0.188	0.067	0.021

The material's refractive index (n) is correlated to the reflectance through the relation [28]:

$$n = \frac{(1+R) + 2\sqrt{R}}{(1-R)} \quad (5)$$

The behavior of the refractive index of NBR-N220 composites in the UV wavelength range, as shown in Figure 6, reveals several key characteristics that are important for practical applications. Initially, as the incident wavelength increases from 200 to 220 nm, the refractive index increases from approximately 1.8 to 2. This initial rising trend suggests enhanced light interaction within the material, which could be attributed to factors such as absorption characteristics, material structure, or electronic transitions that occur within this wavelength range. However, beyond 220 nm, the refractive index decreases monotonically, reaching a value close to 1.5 as the wavelength approaches 300 nm. This decrease may indicate a shift in the dominant optical properties of the composites, possibly reflecting changes in the material's electronic band structure or variations in light scattering and absorption mechanisms. The notable behavior observed around 220 nm could serve as a distinctive feature for applications in optics and photonics, especially in fields that utilize UV light, such as sensor technology, optical filters, or coatings. The ability to manipulate the refractive index in this range can lead to innovations in device design, where precise control over light propagation and interaction is critical. Further investigation into the underlying mechanisms responsible for these changes in refractive index could provide valuable insights for optimizing the performance of NBR-N220 composites in various technological applications.

Figure 6
Variation of refractive index with incident photon wavelength of NBR/N220 composites with different N220 CB concentrations

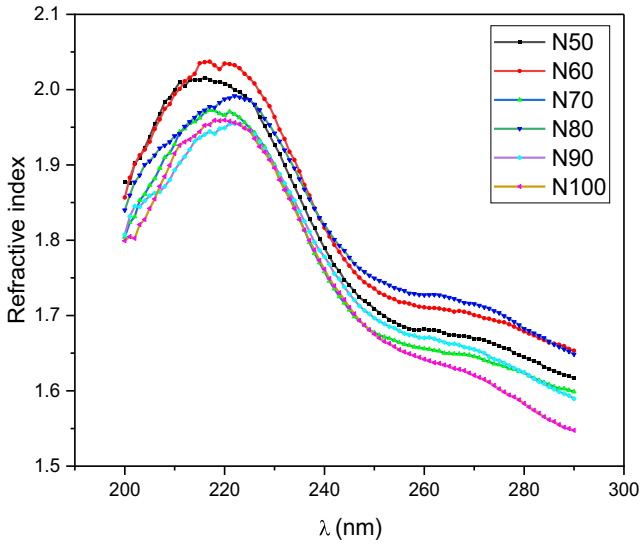

Figure 7
Plot of $(n^2\text{-}1)^{-1}$ versus E^2 for NBR/N220 composites with various CB content to determine the parameters E_0 and E_d according to the WD single effective oscillator model

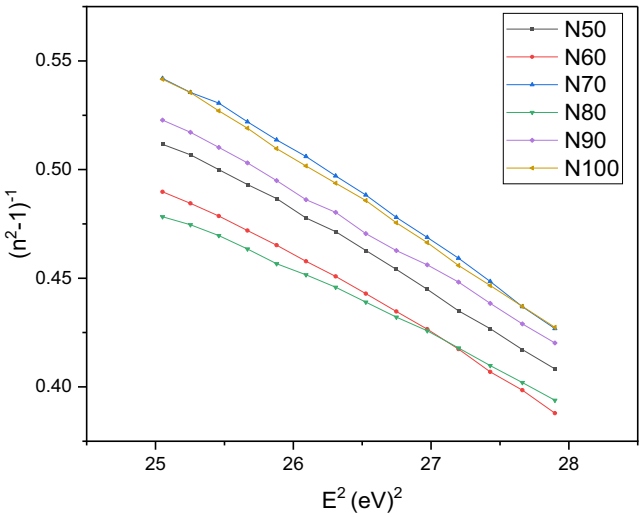

The refractive index dispersion can be characterized using the WD single effective oscillator approach [29, 30]. In the WD model, the refractive index is given by the relation:

$$n^2 = 1 + \frac{E_d E_0}{E_0^2 - E^2} \quad (6)$$

where E_d is the dispersion energy and E_o is the energy of the effective single oscillator.

The energy E_d is the oscillator strength, which indicates the average energy of interband optical transitions, whereas the energy E_o gives an idea about the material's band structure. This is obvious from Figure 7 by plotting $(n^2\text{-}1)^{-1}$ versus E^2 for the investigated NBR/N220 samples. The resultant slope of the straight line is $(-1/E_o E_d)$, while the intercept with the vertical axis equals (E_o/E_d). The calculated parameters E_o and E_d are listed in Table 2.

Table 2
Optical dispersion characteristic parameters of NBR/N220 composites at different CB concentrations as obtained from analysis of WD single oscillator and Sellmeier approaches

Parameter	Samples					
	N50	N60	N70	N80	N90	N100
E_d (eV)	4.401	4.532	3.98	5.296	4.477	3.99
E_0 (eV)	6.311	6.304	6.256	6.508	6.379	6.252
M_{-1}	0.697	0.718	0.636	0.813	0.701	0.638
M_{-3} (eV)$^{-2}$	0.016	0.018	0.016	0.019	0.017	0.016
n_s	1.306	1.316	1.282	1.349	1.307	1.285
λ_0 (μm)	0.198	0.198	0.199	0.193	0.196	0.199
S_0 (μm)$^{-2}$	18.04	18.58	16.14	21.99	18.33	16.41

The dispersion parameters E_o and E_d, obtained from the WD approximation, are utilized to estimate the moments of the optical spectra M_{-1} and M_{-3} as [29, 30]:

$$E_0^2 = \frac{M_{-1}}{M_{-3}},\ E_d^2 = \frac{M_{-1}^3}{M_{-3}} \tag{7}$$

The computed values of E_o and E_d are included in Table 2. The dispersion of the refractive index can also be examined using the Sellmeier equation [31]. This equation employs the Kramers–Kronig relationship, which connects optical absorption with the refractive index, to determine the wavelength-dependent refractive index as follows:

$$\frac{n_s^2-1}{n^2-1} = 1-\left(\frac{\lambda_0}{\lambda}\right)^2 \tag{8}$$

where λ_0 is the average oscillator wavelength and n_s is the static refractive index, also known as the long-wavelength refractive index. The plot of $(n^2\text{-}1)^{-1}$ versus λ^{-2} is shown in Figure 8 for the NBR/N220 composites. From the slope of the straight line, $[\lambda_0^2/(n_s^2\text{-}1)]$, and the intercept with the vertical axis $[1/(n_s^2\text{-}1)]$, one can determine n_s and λ_0 and hence estimate the oscillator length strength $S_o = [(n_s^2\text{-}1)/\lambda_0^2]$. Table 2 gives the estimated values of n_s, Math input error, and S_o for the investigated NBR-N220 composite samples.

3.2. Dielectric properties

The interaction of incident electromagnetic waves and polymeric rubbers is characterized by various dielectric parameters. The static dielectric constant (ε_s), measured at zero or very low frequencies of the incident waves (long wavelengths), can be calculated using the following relation [29]:

$$\varepsilon_s = n_s^2 \tag{9}$$

Based on the values of n_s estimated before, the static dielectric constant is determined for the investigated composites and listed in Table 3.

The dielectric response of a solid when exposed to low-wavelength electromagnetic waves is characterized by its high-frequency dielectric constant (ε_∞). This parameter is connected to the material's refractive index as well as the wavelength of the photons, as described by the following equation [32]:

$$n^2 = \varepsilon_\infty - \left(\frac{e^2}{\pi\, c^2\, \varepsilon_0}\right)\left(\frac{N}{m^*}\right)\lambda^2 \tag{10}$$

where N is the charge carrier density, e is the electronic charge, ε_0 is the permittivity of free space, m^* is the effective mass, and c is the speed of light. Equation (10) establishes a linear relationship between n^2 and λ^2, which is illustrated in Figure 9. The point where the straight line intersects the vertical axis at ($\lambda^2 = 0$) provides the high-frequency dielectric constant, (ε_∞), which is summarized in Table 3 for all composite samples.

Figure 8
Plot of $(n^2\text{-}1)^2$ versus $(\lambda)^{-2}$ of NBR/N220 composites with various CB concentrations to estimate the parameters n_s and λ_0 from the Sellmeier relation

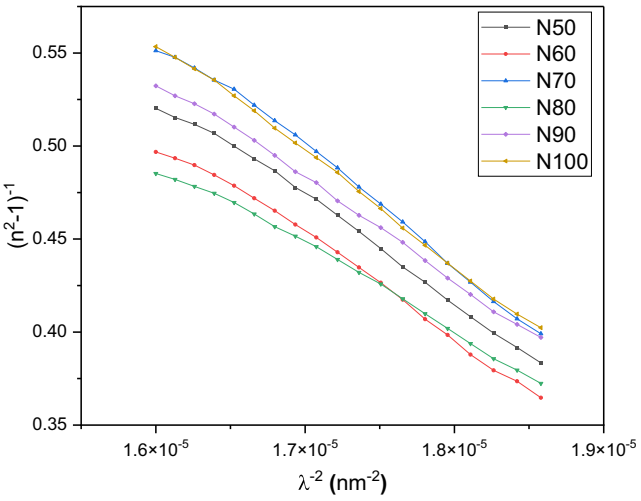

Figure 9
Plot of n^2 versus λ^2 of NBR/N220 composites with different N220 CB concentrations

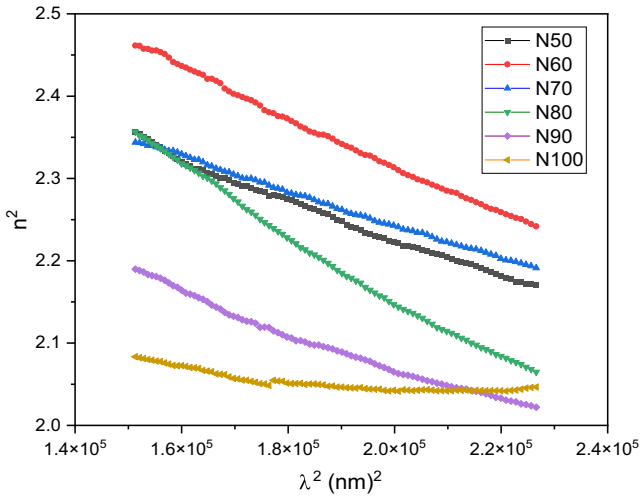

Table 3
Dielectric dispersion parameters, static and high-frequency dielectric constants, and plasma frequency of NBR/N220 composites at different CB concentrations

Parameter	Samples					
	N50	N60	N70	N80	N90	N100
ε_s	1.84	1.72	1.77	1.67	1.84	2.45
ε_∞	2.76	2.89	2.67	2.96	2.48	2.15
$\omega_p(10^{17}$ Hz)	9.2	9.41	9.136	8.583	8.648	8.945

Figure 10
(a) Real part and (b) imaginary part of the dielectric constant versus wavelength of the incident photon for NBR/N220 composites with various CB concentrations

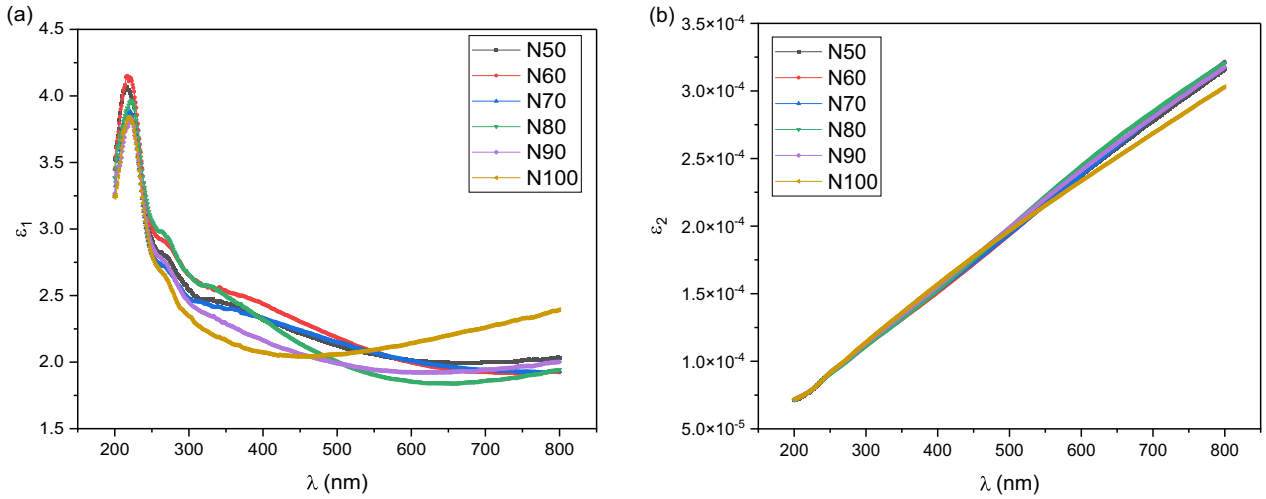

The complex dielectric function (ε^*) of a material with the two components—the real part (ε_1) and the imaginary part (ε_2)—is typically expressed as:

$$\varepsilon^* = \varepsilon_1 - i\varepsilon_2 \tag{11}$$

The real part of the dielectric function represents the material's response to an electromagnetic field in terms of how much it can store energy (dielectric constant), while the imaginary part of the dielectric function is connected to the energy loss in the material due to the electric field (absorption loss), and $i = \sqrt{-1}$ is the imaginary number. The two parts of the dielectric constant are related to the optical parameters by [32]:

$$\varepsilon_1 = n^2 - k^2, \varepsilon_2 = 2nk \tag{12}$$

Dielectric dispersion refers to the frequency-dependent behavior of these components. As frequency changes, both (ε_1) and (ε_2) can change. Frequency dependence can be manifested in several regimes, often characterized by relaxation processes, resonances, and polariton effects. Understanding these aspects is critical for various applications in materials science, electronics, and photonics.

Figure 10(a) and (b) illustrate the variation of the dielectric constants ε_1 and ε_2, respectively, with the incident photon wavelength for the NBR/N220 composites at various CB concentrations. It is noticed from Figure 10 (a) and (b) that the values of ε_1 are greater than those of ε_2. This discrepancy can be attributed to the strong correlation between ε_1 and the refractive index, where k^2 is considerably lower than n^2. Conversely, the lower value of the imaginary dielectric constant could be a result of its dependence on k, leading to a diminished product of $n \times k$.

As a response to the incident waves, the duration required for various conductive sources in NBR/CB composite to revert to their original positions is referred to as the dielectric relaxation time (τ). It plays an important role in both dielectric and mechanical behavior. The correlation between the relaxation time and the dielectric constants is given by [33]:

$$\tau = \frac{\lambda}{c} \frac{(\varepsilon_\infty - \varepsilon_1)}{\varepsilon_2} \tag{13}$$

Figure 11
Dielectric relaxation time τ versus the incident photon wavelength for NBR/N220 CB composites of different CB contents

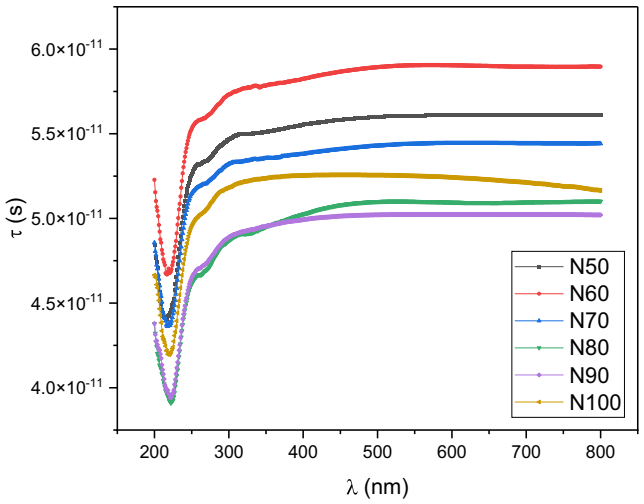

Figure 11 illustrates how the dielectric relaxation time varies with the incident photon wavelength for NBR/N220 composites. Notably, a pronounced decrease in τ is observed at almost 220 nm, which aligns with the region of strong absorption.

Several relaxation processes coexist due to the complex structure of the material: the first process is the dipolar relaxation, which exists in the NBR matrix due to the reorientation of polar groups such as –C≡N and –C=O in NBR under an alternating electric field. Another relaxation type is denoted by interfacial (Maxwell–Wagner–Sillars) relaxation, which is found at NBR/CB interfaces. This is caused by charge accumulation at the interfaces between conductive CB particles and insulating NBR. This is the dominant dielectric relaxation mechanism in NBR/CB composites [34]. Ionic or space-charge relaxation can also be initiated by the trapped charges or impurities due to slow migration or hopping of charges through the composites [35, 36]. Additionally, there can be mechanical (viscoelastic) relaxation attained from the polymer chains associated with chain segment motion, glass transition (α-relaxation), and side-group motion (β-relaxation) [37].

Figure 12
Variation of ε_1 with λ^2 at high wavelength range for NBR/N220 CB composites at different CB concentrations

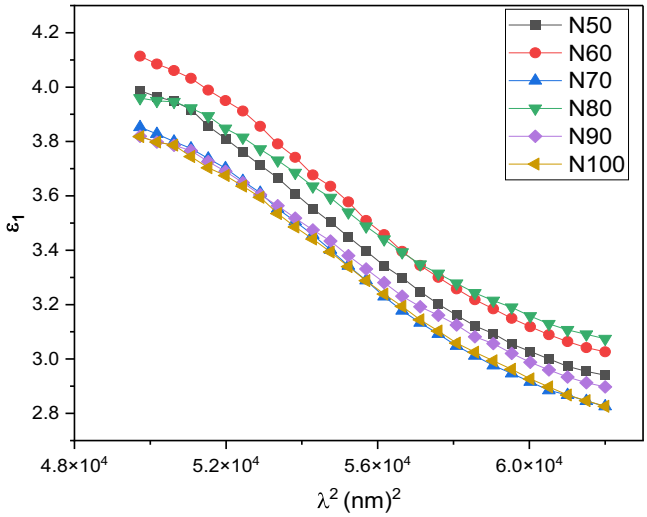

Note: The plasma frequency is calculated from the slope of the straight-line portion.

Rubber by itself is an insulator; it has no mobile charge carriers and thus cannot sustain electron plasma oscillations. Plasma-like collective electron behavior can appear in localized, percolated conductive networks within rubber/CB composites but not in the classical sense of a free electron plasma [38]. When CB is added to the rubber, realistic changes are found. CB is a semimetallic, graphitic material. Its conductivity arises from π–π^* conjugated carbon networks, sp^2 domains interconnected with disordered sp^3 regions, and quantum tunneling or hopping between adjacent CB aggregates. When CB particles are loaded into rubber, at low CB content, the composite remains insulating (isolated CB clusters). At the percolation threshold (~10–20 wt% CB), CB particles form a conductive network, allowing electron hopping or tunneling through the rubber matrix. At high CB content, the system behaves semimetallic, showing frequency-dependent conductivity and plasmon-like absorption in optical or THz spectra [39].

Recent modeling work of polymer–CB interfaces and percolative morphologies explicitly uses generalized Drude descriptions to explain the observed dielectric dispersion in percolative composites [38, 40]. In a rubber/CB complex disordered system, the plasma-like frequency (ω_p) can be calculated based on the wavelength of

Figure 13
Variation of (a) volume energy loss function, (b) surface energy loss function, and (c) loss tangent, with the incident photon wavelength for NBR/N220 composites of various CB contents

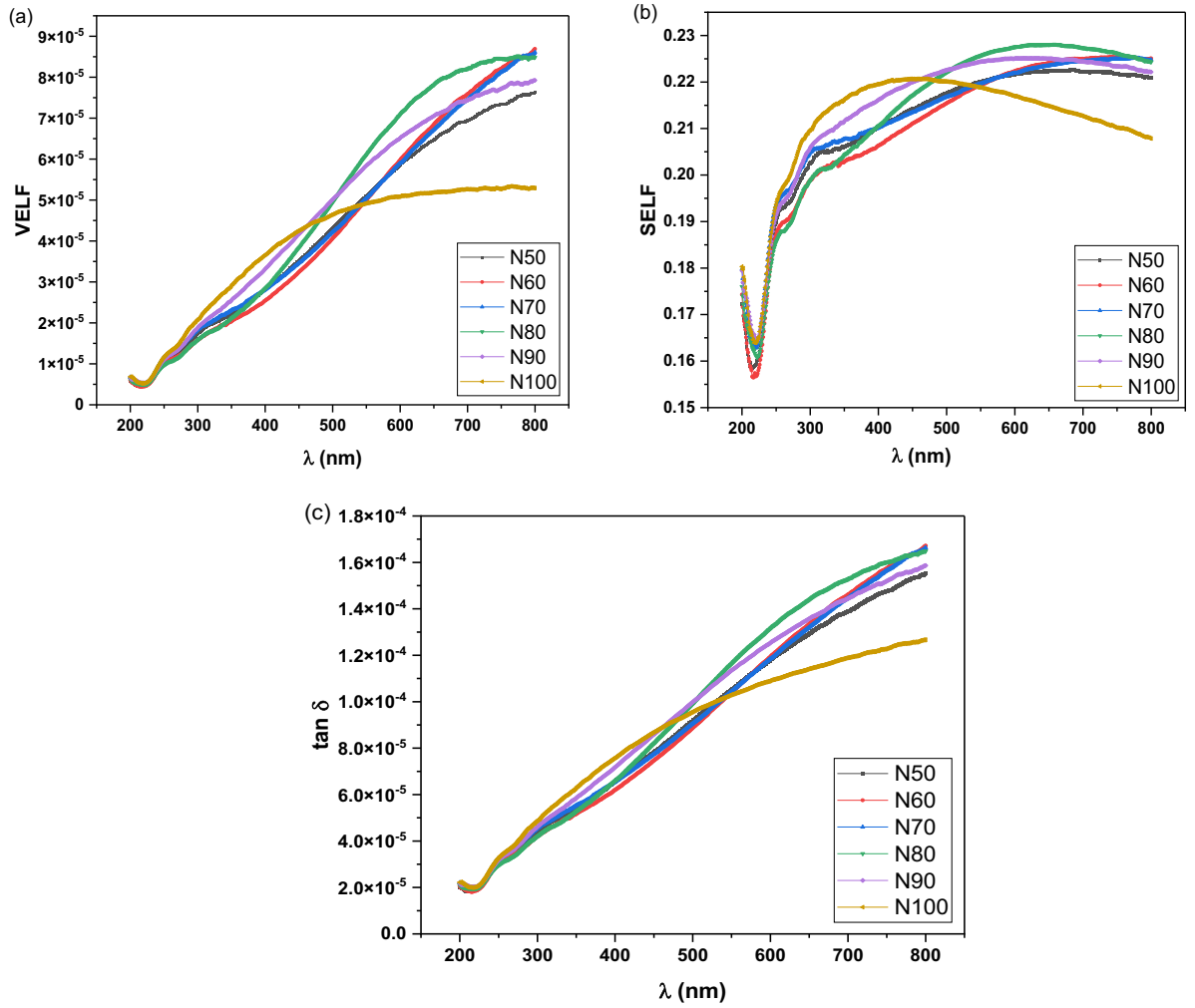

the incident wave, the high-frequency dielectric constant, and the real part of the dielectric constant as [41]:

$$\varepsilon_1 = \varepsilon_\infty - \frac{\omega_p^2 \lambda^2}{c^2} \quad (14)$$

The plasma frequency, then, can be determined by plotting ε_1 versus λ^2, at high wavelength range; this is illustrated in Figure 12. The slope of the fitted straight line equals ($-\omega_p^2/c^2$) from which ω_p is evaluated. The result is listed in Table 3. Several studies show that percolative CB composites can be interpreted as collective/plasmonic oscillations at ultra-low plasma frequencies. This supports the notion of network-confined plasmon-like modes rather than a bulk metal plasma [41].

When the material is subjected to electromagnetic radiation, the rapid oscillation of charge carriers within the bulk and on the surface of the solid leads to energy loss that is linked to the optical properties and dielectric function. The dielectric loss is characterized by three functions: volume energy loss function (VELF), surface energy loss function (SELF), and loss tangent (tan δ). These parameters depend on the dielectric constant and can be determined using the following relationships [42]:

$$VELF = \frac{\varepsilon_2}{\varepsilon_1^2 + \varepsilon_2^2}, \; SELF = \frac{\varepsilon_1}{(\varepsilon_1 + 1)^2 + \varepsilon_2^2}, \; tan\delta = \frac{\varepsilon_2}{\varepsilon_1} \quad (15)$$

Figure 13 shows how these loss functions vary with the incident photon wavelength for NBR-N220 composite samples. It is evident from the figure that up to about 220 nm (the strong absorption zone), the dielectric loss functions rapidly decrease with increasing incident photon wavelength and then increase steadily [43].

4. Conclusion

NBR composites filled with varying contents of N220 CB were fabricated via conventional mixing and vulcanized at 150 °C under 15 MPa. Optical characterization revealed strong ultraviolet absorption that intensified with increasing CB loading, reflecting enhanced light–filler interactions and network formation. The optical and dielectric parameters analyzed using the Urbach, WD, and Sellmeier models confirmed that the addition of N220 significantly modifies the electronic structure and optical response of the NBR matrix. The observed variations in absorption coefficient, optical band gap, refractive index, and dielectric constant underscore the tunability of these composites for potential use in flexible electronic and optoelectronic devices. Further studies are recommended to elucidate the correlation between mechanical reinforcement and optical functionality to enable targeted performance optimization of NBR/CB systems.

Ethical Statement

This study does not contain any studies with human or animal subjects performed by any of the authors.

Conflicts of Interest

The authors declare that they have no conflicts of interest to this work.

Data Availability Statement

Data are available from the corresponding author upon reasonable request.

Author Contribution Statement

K. Alfaramawi: Conceptualization, Formal analysis, Resources, Writing – review & editing. **S. Abboudy:** Formal analysis, Resources, Data curation, Writing – review & editing, Visualization, Supervision, Project administration. **L. Abulnasr:** Formal analysis, Investigation, Data curation, Writing – review & editing. **S. Ebrahim:** Investigation, Writing – review & editing. **Ahlam K. Yousif:** Methodology, Data curation, Writing – original draft.

References

[1] Jiang, B., Jia, X., Wang, Z., Wang, T., Guo, F., & Wang, Y. (2019). Influence of thermal aging in oil on the friction and wear properties of nitrile butadiene rubber. *Tribology Letters*, *67*(3), 86. https://doi.org/10.1007/s11249-019-1201-8

[2] Mirsafai, S., Torabi, K., Ashrafi, M., & Hamadanian, M. (2020). Tensile strength and elongation of NBR/PVC/CuFe2O4 magnetic nanocomposites: A response surface methodology optimization. *Bulletin of Materials Science*, *43*(1), 101. https://doi.org/10.1007/s12034-020-2066-z

[3] Rahaman, M., Gupta, P., Hossain, M., Periyasami, G., & Das, P. (2023). Effect of carbons' structure and type on AC electrical properties of polymer composites: Predicting the percolation threshold of permittivity through different models. *Colloid and Polymer Science*, *301*(8), 1001–1019. https://doi.org/10.1007/s00396-023-05120-2

[4] Huang, L., Tao, X., Wei, T., & Li, Z. (2024). Microstructure effect analysis of carbon black-filled rubber composites. *International Journal of Numerical Methods for Calculation and Design in Engineering*, *40*(1), 1–15. https://doi.org/10.23967/j.rimni.2024.01.002

[5] Wang, Y., Jiang, W., Zhu, K., Wu, L., & Chen, L. (2024). Effects of carbon black surface modification on the morphology and properties in blends with natural rubber studied with high-resolution x-ray computed tomography. *Macromolecular Materials and Engineering*, *309*(5), 2400019. https://doi.org/10.1002/mame.202400019

[6] Chakraborti, S., Banerjee, P. S., Basu, D., Wießner, S., Heinrich, G., Das, A., & Banerjee, S. S. (2025). Elastomers for soft electronics: A review from the material's perspective. *Advanced Engineering Materials*, *27*(9), 2402458. https://doi.org/10.1002/adem.202402458

[7] Zou, M., Gao, W., Li, Z., Liu, B., Li, B., Liu, K., & Liu, J. (2024). Hybrid carbon black/silica reinforcing system for high-performance green tread rubber. *Polymers*, *16*(19), 2762. https://doi.org/10.3390/polym16192762

[8] Taha, T. A., Hendawy, N., El-Rabaie, S., Esmat, A., & El-Mansy, M. K. (2019). Effect of NiO NPs doping on the structure and optical properties of PVC polymer films. *Polymer Bulletin*, *76*(9), 4769–4784. https://doi.org/10.1007/s00289-018-2633-2

[9] Alfaramawi, K. (2018). Optical characteristics of butyl rubber loaded with general purpose furnace (GPF) carbon black. *Materials Research Express*, *5*(6), 066202. https://doi.org/10.1088/2053-1591/aac7fa

[10] Samthong, C., Kunanusont, N., Deetuam, C., Wongkhan, T., Supannasud, T., & Somwangthanaroj, A. (2019). Effect of acrylonitrile content of acrylonitrile butadiene rubber on mechanical and thermal properties of dynamically vulcanized poly(lactic acid) blends. *Polymer International*, *68*(12), 2004–2016. https://doi.org/10.1002/pi.5912

[11] Parvathi, K., Bahuleyan, B. K., & Ramesan, M. T. (2022). Enhanced optical, thermal and electrical properties of chlorinated natural rubber/zinc ferrite nanocomposites for flexible electrochemical devices. *Journal of Macromolecular Science, Part A*, *59*(7), 466–479. https://doi.org/10.1080/10601325.2022.2080076

[12] Rejani, P., & Beena, B. (2013). Structural and optical properties of polyindole-manganese oxide nanocomposite. *Indian Journal of Advances in Chemical Science*, *2*(3), 244–248.

[13] Naser, H., Shanshool, H. M., Mohammad, S. M., Hassan, Z., Abbas, A. M. A., Abed, S. M., & Sifawa, A. A. (2024). Optical properties of polymers mixed with zinc oxide, silver, and aluminum nanoparticles. *Journal of Materials Science: Materials in Electronics*, *35*(23), 1582. https://doi.org/10.1007/s10854-024-13346-1

[14] Naser, H., Mohammad, S. M., Shanshool, H. M., Hassan, Z., Mohammed, A. A. A., & Rajamanickam, S. (2024). Evaluation and analyzing the linear optical properties of polymer/Al-Ag-ZnO nanocomposites. *Plasmonics*, *19*(6), 3043–3058. https://doi.org/10.1007/s11468-024-02223-6

[15] Naser, H., Mohammad, S. M., Shanshool, H. M., Hassan, Z., & Hazeem, Z. A. (2024). Energy band gap investigation of Al nanoparticles/polystyrene nanocomposite foils. *International Journal of Nanotechnology*, *21*(4–5), 313–323. https://doi.org/10.1504/IJNT.2024.141762

[16] Alam, M. N. (2024). Advances in functional rubber and elastomer composites. *Polymers*, *16*(12), 1726. https://doi.org/10.3390/polym16121726

[17] ASTM International. (2012). *ASTM D3182-07: Standard practice for rubber – Materials, equipment, and procedures for mixing standard compounds and preparing standard vulcanized sheets*. Retrieved from: https://store.astm.org/d3182-07.html

[18] Alfaramawi, K., Abboudy, S., Abulnasr, L., Haridy, A. O., & Alexandria. (2022). Synthesis and characterization of EPDM loaded with zinc/carbon black hybrid filler. *KGK Kautschuk Gummi Kunststoffe*, *75*(5), 39–47.

[19] Gesesse, G. D., Gomis-Berenguer, A., Barthe, M.-F., & Ania, C. O. (2020). On the analysis of diffuse reflectance measurements to estimate the optical properties of amorphous porous carbons and semiconductor/carbon catalysts. *Journal of Photochemistry and Photobiology A: Chemistry*, *398*, 112622. https://doi.org/10.1016/j.jphotochem.2020.112622

[20] Kubelka, P., & Munk, F. (1931). Ein beitrag zur optik der farbanstriche [A contribution to the appearance of paint finishes]. *Zeitschrift für Technische Physik*, *12*(11a), 593–601. Retrieved from: https://www.researchgate.net/profile/Rob-Keller/post/Dismissed_journals-articles_database/attachment/6255b567f711e16f6a914024/AS%3A1144091874213889%40164978167321/download/KubelkaP.andMunkF.1931EinBeitragZurOptikDerFarbanstriche.ZeitschriftfrTechnischePhysik12593-601..pdf

[21] Sıdır, Y. G., & Sıdır, İ. (2025). The optical properties, UV-Vis. absorption and fluorescence spectra of 4-Pentylphenyl 4-n-benzoate derivatives in different solvents. *Journal of Fluorescence*, *35*(9), 8269–8287. https://doi.org/10.1007/s10895-025-04154-9

[22] Lekishvili, N., Nadareishvili, L., Zaikov, G., & Khananashvili, L. (2023). *Polymers and polymeric materials for fiber and gradient optics*. USA: CRC Press. https://doi.org/10.1201/9780429070686

[23] Gavrilenko, V. I., & Ovechko, V. S. (2023). *Fundamentals of the optics of materials: Tutorial and problem solving*. USA: Jenny Stanford Publishing. https://doi.org/10.1201/9781003256946

[24] Alfaramawi, K. (2018). Optical and dielectric dispersion parameters of general purpose furnace (GPF) carbon black reinforced butyl rubber. *Polymer Bulletin*, *75*(12), 5713–5730. https://doi.org/10.1007/s00289-018-2353-7

[25] Doma, A. S., Kamoun, E. A., Abboudy, S., Belal, M. A., Khattab, S. N., & El-Bardan, A. A. (2019). Compatibilization of vulcanized SBR/NBR blends using Cis-polybutadiene rubber: Influence of blend ratio on elastomer properties. *European Journal of Engineering and Technology Research*, *3*(12), 135–143. https://doi.org/10.24018/ejeng.2018.3.12.958

[26] Zhang, T., Zheng, Z., Zhang, M., Li, S., Huang, H., & Zhang, Z. (2024). Investigation of dielectric properties and conductivity of polyvinyl chloride composites by terahertz time-domain spectroscopy. *Polymer Testing*, *134*, 108446. https://doi.org/10.1016/j.polymertesting.2024.108446

[27] Kumar, K., Kumar, Y., & Awana, V. P. S. (2023). Weak anti-localization effect in topological Ni3In2S2 single crystal. *Journal of Materials Science: Materials in Electronics*, *34*(36), 2302. https://doi.org/10.1007/s10854-023-11756-1

[28] Schubert, E. F. (2022). *Physical foundations of solid-state devices*. USA: E. Fred Schubert.

[29] DrDomenico, M., & Wemple, S. H. (1969). Oxygen-octahedra ferroelectrics. I. Theory of electro-optical and nonlinear optical effects. *Journal of Applied Physics*, *40*(2), 720–734. https://doi.org/10.1063/1.1657458

[30] Wemple, S. H., & DiDomenico, M. (1969). Optical dispersion and the structure of solids. *Physical Review Letters*, *23*(20), 1156–1160. https://doi.org/10.1103/PhysRevLett.23.1156

[31] Joshi, J. H., Khunti, D. D., Joshi, M. J., & Parikh, K. D. (2017). Penn model and Wemple-DiDomenico single oscillator analysis of cobalt sulfide nanoparticles. *Functional Oxides and Nanomaterials*, *1837*(1), 040033. http://dx.doi.org/10.1063/1.4982117

[32] El Hachmi, A., & Manoun, B. (2023). Complex dielectric, electric modulus, impedance, and optical conductivity of Sr3−xPbxFe2TeO9 (x = 1.50, 1.88 and 2.17). *International Journal of Materials Research*, *114*(2), 100–111. https://doi.org/10.1515/ijmr-2022-0189

[33] El-naggar, A. M., Heiba, Z. K., Mohamed, M. B., Kamal, A. M., Lakshminarayana, G., & Abd-Elkader, O. H. (2022). Effect of MnS/ZnS nanocomposite on the structural, linear and nonlinear optical properties of PVA/CMC blended polymer. *Optical Materials*, *128*, 112379. https://doi.org/10.1016/j.optmat.2022.112379

[34] Sun, H., Zhang, H., Liu, S., Ning, N., Zhang, L., Tian, M., & Wang, Y. (2018). Interfacial polarization and dielectric properties of aligned carbon nanotubes/polymer composites: The role of molecular polarity. *Composites Science and Technology*, *154*, 145–153. https://doi.org/10.1016/j.compscitech.2017.11.008

[35] Kim, G.-H., Moon, Y.-I., Jung, J.-K., Choi, M.-C., & Bae, J.-W. (2022). Influence of carbon black and silica fillers with different concentrations on dielectric relaxation in nitrile butadiene rubber investigated by impedance spectroscopy. *Polymers*, *14*(1), 155. https://doi.org/10.3390/polym14010155

[36] Li, B., Polizos, G., & Manias, E. (2022). Interfacial effects on the dielectric properties of elastomer composites and nanocomposites. In A. Schönhals & P. Szymoniak (Eds.), *Dynamics of composite materials* (pp. 225–249). Springer International Publishing. https://doi.org/10.1007/978-3-030-89723-9_8

[37] Rahaman, M. (2023). Superior mechanical, electrical, dielectric, and EMI shielding properties of ethylene propylene diene monomer (EPDM) based carbon black composites. *RSC Advances*, *13*(36), 25443–25458. https://doi.org/10.1039/D3RA04187E

[38] Brosseau, C. (2024). Modeling the interface between phases in dense polymer-carbon black nanoparticle composites by dielectric spectroscopy: Where are we now and what are the opportunities? *Macromolecular Theory and Simulations*, *33*(3), 2400009. https://doi.org/10.1002/mats.202400009

[39] Moon, Y., Lee, H., Jung, J., & Han, H. (2023). Direct visualization of carbon black aggregates in nitrile butadiene rubber by THz near-field microscope. *Scientific Reports*, *13*(1), 7846. https://doi.org/10.1038/s41598-023-34565-2

[40] Huang, M., Tunnicliffe, L. B., Liao, S., Yang, B., Yan, H., & Busfield, J. J. C. (2023). Broadband dielectric characterization of carbon black–reinforced natural rubber. *Rubber Chemistry and Technology*, *96*(4), 656–666. https://doi.org/10.5254/rct.23.76983

[41] Shi, G., Sun, X., & Liu, Y. (2024). Percolation-triggered negative permittivity in nano carbon powder/polyvinylidene fluoride composites. *Molecules*, *29*(16), 3862. https://doi.org/10.3390/molecules29163862

[42] Cai, J., Wang, J., Li, F., Zhang, X., Feng, B., Yu, Z., & Li, Y. (2025). Preparation of BiVO4 films and modulation of their photocatalytic properties by pulsed laser deposition, magnetron sputtering, and atomic layer deposition. *ACS Applied Electronic Materials*, *7*(12), 5331–5353. https://doi.org/10.1021/acsaelm.5c00566

[43] Hassanien, A. S., Sharma, I., & Sharma, P. (2023). Optical and dispersion studies of thin S35-xGe15SnxTe50 films: Assessment of some physical parameters of samples. *Physica Scripta*, *98*(4), 045911. https://doi.org/10.1088/1402-4896/acc2f9

How to Cite: Alfaramawi, K., Abboudy, S., Abulnasr, L., Ebrahim, S., & Yousif, A. K. (2026). Evaluation and Characterization of the Optical Properties of NBR Rubber/N220 Granular Carbon Black Composites. *Journal of Optics and Photonics Research*. https://doi.org/10.47852/bonviewJOPR62027361